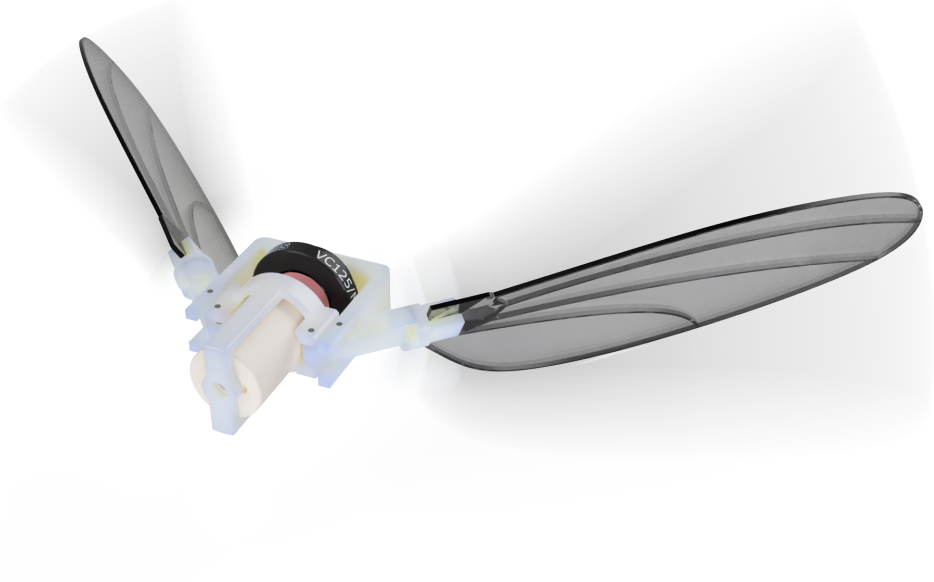

Systems Design of an Insectoid Propulsion System

Bachelor Thesis at The Department of Mechanics and Maritime Sciences (M2)

Elias Hedberg
Simon Karlsson
Christofer Nilsson
Anton Wikström

DEPARTMENT OF MECHANICS AND MARITIME SCIENCES
CHALMERS UNIVERSITY OF TECHNOLOGY
Gothenburg, Sweden 2024
www.chalmers.se

Bachelor Thesis 2024

Systems Design of an Insectoid Propulsion System

ELIAS HEDBERG
SIMON KARLSSON
CHRISTOFER NILSSON
ANTON WIKSTRÖM

CHALMERS

Department of Mechanics and Maritime Sciences
Chalmers University of Technology
Gothenburg, Sweden 2024

Systems Design of an Insectoid Propulsion System
ELIAS HEDBERG
SIMON KARLSSON
CHRISTOFER NILSSON
ANTON WIKSTRÖM

Supervisor: Arion Pons, Department of Mechanics and Maritime Sciences
Examiner: Niklas Andersson, Department of Mechanics and Maritime Sciences

Bachelor's Thesis 2024
Department of Mechanics and Maritime Sciences
Chalmers University of Technology
SE-412 96 Gothenburg
Telephone +46 31 772 1000

Cover: A 3D render of the final design used in the project.

Typeset in LaTeX
Printed by Chalmers Reproservice
Gothenburg, Sweden 2024

Systems Design of an Insectoid Propulsion System
ELIAS HEDBERG
SIMON KARLSSON
CHRISTOFER NILSSON
ANTON WIKSTRÖM
Department of Mechanics and Maritime Sciences
Chalmers University of Technology

Abstract

A flapping wing micro aerial vehicle (MAV) is a small unmanned vehicle inspired by insects and or birds. These have become a trending area of research and development within the MAV community due to their potential of unprecedented flight capabilities. Most notable of such capabilities being the efficient hovering, quick change of direction and tiny weight and size associated with flying insects. However, the design imposes mechanical challenges due to its size and the dynamics of the flapping wing design. Here we show that by incorporating a systems design approach the number of promising designs of a MAV propulsion system can be limited, and a general direction of further improvement can be found. Tests showed that maximum power for medium to large sized, fruit fly inspired, wings on the insectoid propulsion system were achieved with a soft spring and lower frequency, while smaller wings produced most power when coupled with a stiffer spring and higher frequency. Our result show how a complex multi-discipline problem can be broken down into smaller parts and solved separately while still improving the system as a whole. Using this method the weight of the body of the original prototype was decrease by 84.5% to 3.72 g and the wing's weight was decreased by 48% to 1.32 g. Further the generated thrust from the propulsion system was increased to 1.39 g under continuous operation at 10 V and reaching 4.03 g of thrust under temporary operation at 30 V. We anticipate the findings in this report will act as a starting point for further improvements of the design of flapping wing MAV propulsion systems.

Keywords: micro areal vehicle, flapping wing, insectoid, drone, Voice coil actuator, propulsion system.

Acknowledgements

We would like to give our thanks to our supervisor for the project, Arion Pons, Assistant Professor at Chalmers University of Technology, whose guidance, interest and expertise has been of substantial help for the completion of the project. His dedication to teaching, constructive feedback and assistance during the project has greatly contributed to our understanding and learning of the subject matter.

Elias Hedberg, Simon Karlsson, Christofer Nilsson & Anton Wikström
Gothenburg, May 2024

List of Acronyms

Below is the list of acronyms that have been used throughout this thesis listed in alphabetical order:

ABS	Acrylonitrile Butadiene Styrene
CAD	Computer Aided Design
DC	Direct Current
FDM	Fused Deposition Modelling
fps	Frames per second
MAV	Micro Aerial Vehicle
PCB	Printed Circuit Board
PLA	Polylactic acid
PTFE	Polytetrafluoreten
PVA	Polyvinyl alcohol
PWM	Pulse Width Modulation
SLA	Stereolithography
STL	Standard Tessellation Language
TPU	Thermoplastic polyurethane
UART	Universal Asynchronous Receiver/Transmitter
VCA	Voice Coil Actuator

Nomenclature

Below is the nomenclature of variables utilised throughout this thesis.

Variables

F	Force (N)
B	Flux density (T)
I	Current (A)
f_{wing}	Wingbeat frequency (Hz)
φ	Wing position-angle (°)
α	Angle of attack (°)
θ	Stroke amplitude (°)
f_{pwm}	Pulse width modulation frequency (Hz)
res_{pwm}	Pulse width modulation resolution (bits)

Contents

List of Figures

List of Tables

1

Introduction

1.1 Background

Nobody who has swatted a fly, trod through a cloud of midges, or been bitten by a mosquito has failed to be impressed, and possibly infuriated, by the extraordinary capabilities of flying insects: their manoeuvrability, endurance, and tiny scale. Being able to replicate these capabilities in an insectoid micro-air-vehicle (MAV) would represent a significant advance in the capabilities of MAV systems. However, designing insectoid MAVs is a complex task: conventional motors and transmissions are not well-suited for generating the complex oscillating wingbeat patterns required for insectoid propulsion. Instead, significant mechanical and systems design effort is required in order to develop dedicated oscillatory drivetrains for these propulsion systems.[1] An example of an existing MAV is the RoboBee from Harvard University, designed in 2009 [2]. The RoboBee mimics the flight of flies and is only as big as a quarter. Its body is integrated with an actuator that generates movement for a rigid pair of wings to fly. The entire assembly is a compliant design aimed at minimising rigid hinges and reducing weight.

What makes the development of an insectoid MAV especially interesting is the potential to create lighter and smaller drones while maintaining performance at the same level. Another reason to develop an insectoid MAV is its capability to quickly change direction and hover. This project is based on an existing insectoid propulsion system prototype, which will serve as the foundational concept to be improved or renewed. The initial design of the insectoid propulsion system originated from an earlier project conducted by two amanuensis students at Chalmers, who independently developed the wing design and actuator assembly. This provided a foundational model for the project, albeit one that was somewhat cumbersome and inefficient. However, it served as an excellent starting point. The initial prototype features a body with a compliant design, employing no rigid joints for movement, instead, the flexion of the material generates movement between joints. The wing design for the initial insectoid propulsion system is biomimetic, drawing inspiration from a fruit fly. Previous unfinished iterations of the wings included a swooping design, resembling a sail to catch a vortex and generate lift, while other designs featured solid wings utilising a hinge to sweep and change direction, similar to the current design of the insectoid propulsion system.

1.2 Purpose

The project aims to enhance an initial prototype of an insectoid micro-air-vehicle propulsion system from a previous project, as depicted in Figure 1.1, with the objective to increase lift. To take the prototype closer to take off, a higher lift-to-weight ratio is required while maintaining reliability at a level sufficient for benchmarking. The result of this projects will manifest in the form of a new prototype with improved weight optimisation, mechanical durability, wing design and wing movement.

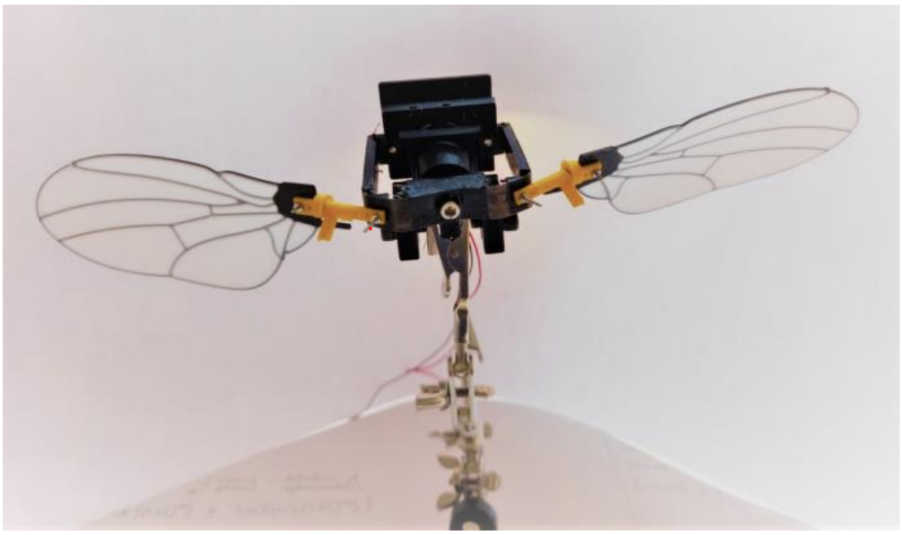

Figure 1.1: The initial prototype of the insectoid propulsion system.

1.3 Problem

The wings and actuator components of the initial propulsion system prototype were developed separately and had not been operated together previously, thus not generating any lift. Therefore there is a need for integration studies of said propulsion system prototype. Subsequently the problem at hand is to increase the lift by integrating the different subsystem as well as improving the lift-to-weight ratio. The lift-to-weight ratio is a problem of optimising the weight while keeping structural integrity and increasing lift without increasing the weight and size. To achieve this, improvements on the following parts is necessary:

A) The control electronics includes a pulse-width modulation (PWM) generator, a motor driver and a voice coil actuator (VCA). The drive electronics is an optimisation problem where finding the optimal signal shape and type as well as properly specifying the requirements of the voice coil actuator is critical.

B) The transmission mechanism includes a 3D-printed mechanism translating the VCAs linear actuation into wing beat oscillation, and a passive wing twist hinge based around micro roller bearings. The transmissions mechanism is a part of the system that need to be reevaluated to increase the stroke amplitude (see 2.1.5). The choice of material is an important design aspect that can be optimised to ensure structural integrity while reducing weight and size.

C) The wings is desired to be lightweight to accomplish lift and stability. The challenge in the design of the wings lies in finding the optimal wing shape and size while choosing a material that is light and has the optimal rigidity.

1.4 Project boundaries

The project will be limited to working on improvements regarding weight, translating linear movement to the complex oscillating wing movement, durability, electronics and software improvements. The project is set to be completed in one semester, which limits the time for testing and development. The project will adjust to the time period to complete all the set tasks on deadline. The construction of the insectoid propulsion system will be manufactured at makerspaces and labs at Chalmers University, primarily Chalmers FUSE, CASE Lab and 3Dteamet's workshop. The labs availability of tools and processes will affect the quality of the propulsion system which could decrease the quality compared to the goal. The construction is not planned to use any simulations to evaluate the flow dynamics of the propulsion system because of the limited time period of the project. The propulsion system will not have any onboard control systems to control the flight of the propulsion system. The control system will be off board when testing and only the mechanical parts of the propulsion system will be bench-marked. Further more the project will be limited by only using the Thorlabs VC125/M VCA [3] to facilitate ongoing research regarding the drivetrain.

1.5 Ethical considerations

The development of an insectoid MAV propulsion system does in itself not cause any direct harm or benefit. However, a insectoid MAV may be used in ways that could cause harm. It could be used to infringe on the privacy of citizens if equipped with a microphone or camera. The MAV could also be used to transport illicit objects. However these problems are shared by all unmanned air vehicles and as such, can not be attributed to the insectoid propulsion system. Therefore, our findings won't cause any harm already done by existing technology.

2
Theory

2.1 Mechanical principles of insectoid flight

The theory and mechanics of insect flight and insectoid MAVs is a complex and diverse field, crossing into multiple disciplines. The following section will however provide some necessary basic and general understanding of the subjects.

2.1.1 Insectoid flight

First, we consider the biomechanical basis of insect flight. In humans, skeletal muscle contraction is controlled by calcium ions stored in the *sarcoplasmic reticulum* which is located inside the muscle cell [4]. The charge of the calcium ions enable rapid deployment and, as a consequence, rapid contraction of skeletal muscles. However, a limitation arises when the muscle subsequently is to be relaxed. To relax the muscle the calcium ions has to be pumped back into the *sarcoplasmic reticulum* against its electrochemical gradient. This illustrates why skeletal muscles are not an ideal fit for the frequencies required to achieve insect flight. The muscles used by insects in flight have different properties in order to provide both fast activation and de-activation of the muscle. In insects, each muscle contraction does not require prior neuron firing, and are therefore referenced to as asynchronous flight muscles [4]. Instead, the muscle contraction and relaxation is controlled in a more mechanical fashion. When the muscle is rapidly stretched, cross-bridges activate and the muscle generates power, the subsequent rapid shortening of the muscles disables these connections and the cycle repeats. This enables the wings to be flapped at a higher frequency than what skeletal muscles are able to accomplish.

2.1.2 Compliant and Rigid Mechanisms

In order to transmit the linear driving motion to the flapping wings, a transmission mechanism is needed. The transmission can either be compliant or non-compliant, also called rigid. A good explanation of compliant mechanisms comes from Larry L. Howell in 21st century kinematics: "Compliant mechanisms gain their motion from the deflection of elastic members. ... Because compliant mechanisms gain their motion from the constrained bending of flexible parts, they can achieve complex motion from simple topologies."[5] while the traditional (rigid) mechanisms instead use "rigid parts connected at articulating joints (such as hinges, axles, or bearings), which usually requires assembly of components and results in friction at the connecting surfaces."[5] Howell continues with a point that summarises the relevance

of compliant mechanisms for development of insectoid propulsion systems, "Compliant mechanisms also offer an opportunity to achieve complex motions within the limitations of micro- and nano-fabrication. Nature provides an example of how to effectively create controlled motion. Most moving components in nature are flexible instead of stiff, and the motion comes from bending the flexible parts instead of rigid parts connected with hinges (for example, consider hearts, elephant trunks, and bee wings)" [5].

2.1.3 Spring loaded mechanism

Oscillating motion requires a significant amount of work in order to constantly flip the direction of movement. This is because the reciprocating wing motion necessary for flapping wings can be, according to Hines et al. [6], "quite power intensive as it is not only aerodynamic drag that must be overcome, but also the inertia of the constantly oscillating wing and accompanying mechanisms. Insects such as fruit flies drive their wings at mechanical resonance to combat this effect". Therefore resonance can be exploited in a mechanical system to generate large wing stroke amplitudes and to avoid reactive losses to the inertia of flapping wings [1]. In order to achieve resonance for a system, a spring element can be introduced. In theory for every combination of wings and linkage system its possible to tune the stiffness of a spring elements until it resonates at the flapping frequency. Insects utilise this principle as seen in figure 2.1.

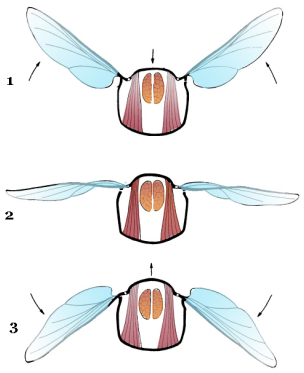

Figure 2.1: Illustration of the muscles contraction inside a fruit fly. Notice the outer shell working as spring when the muscles contract.[7]

2.1.4 Bistable mechanisms

Another way to minimise reaction losses and maximise power output is to make use of bistable mechanisms. In ""Clicking" Compliant Mechanism for Flapping-Wing Micro Aerial Vehicle" the authors Chin and Lau [8] explains the principle of bistability and its advantages in wing clapping mechanism with a comparison to Dipteras (two winged insects): "Diptera adopt a "click" mechanism, which involves buckling of the flexure joints, to induce a large wing stroke at high speed. The main characteristic of 'clicking' mechanism in Diptera is that there are two extremes position of travel where the wing either sets at the top dead position or the bottom

dead position. When the wing is moved just slightly from one extreme position, it will recoil back to the same position upon release. However, when moved beyond the midpoint of the two extreme positions, the wing would click to the other extreme upon release" [8]. Chin and Lau further states that mathematical analysis by Tang and Brennan in "On the dynamic behaviour of the “click” mechanism in dipteran flight" [9] suggests that, the clicking mechanism is better than resonance effect in achieving a faster and large wing stroke and producing higher thrust give the same input.

2.1.5 Kinematic parameters

The flight properties of any flapping wing propulsion system depends on the combination of a substantial amount of different parameters. A few such parameters, those that will be taken into consideration in this project, are stroke amplitude, angle of attack, wingbeat frequency, mass, inertia and natural frequency of both swinging and bending bodies.

Stroke amplitude is the measurement of the wingbeat sweep given in degrees, in this paper it is refered to as θ and defined as the angle between the rearmost and foremost position of the wings during flapping as illustrated in figure 2.2. The plane within which this angle is spanning is called stroke plane.

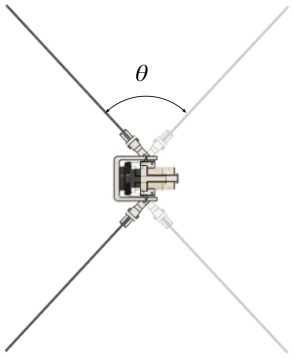

Figure 2.2: Example of stroke amplitude

Angle of attack α is the angle at which the wing nominally sweeps through the air measured as the angle between the plane of the wing and the stroke plane.

Wingbeat frequency describes the number of wingbeats. One wingbeat referring to one forward and one backward swing of a wing, per second and is measured in Hz.

Natural frequency refers to the frequency where resonance occurs and can be desirable in regards to natural flapping frequency and pitching of wings while being undesirable in regards to for example flexing of the wing.

2.2 Electronics components

To drive the propulsion system, a row of electronic components are used to achieve the desired driving motion and accompanying suitable drive signals. This can be achieved in many ways, therefore the theory, functionality and usage of the electronics behind how it was achieved in this project will be described.

2.2.1 Voice Coil Actuator

Voice coil actuators are one of the kinds of actuators that can be used as an 'artificial muscle' to power insectoid flight, and that its the type of actuator this prototype uses. Voice coil actuators are one of the simplest types of motor as they only consist of two separate parts; a magnetic housing with a permanent magnetic core and a coil [10]. It generates a linear force when current flows through the coil and the induced magnetic field interacts with the permanent magnetic field [11]. Which means that the VCA follows Lorentz' force equation 2.1.

$$F = B \times I \tag{2.1}$$

Voice coil actuators also provide a linear motion which removes the need of a translation mechanism which in turn reduces the complexity of the system. Another reason to study the use of VCA:s is that they provide almost constant force, with small variations at the end points. [10] The VC125/M [3] VCA (see figure 2.3) used in this project can provide a constant linear force at micrometer level at frequencies up to 2 kHz, while at millimeter level it's able to operate at 30 Hz (Thorlabs support, personal communication, March 2, 2024). The Thorlabs VC125/M [3] VCA is designed for use cases where high precision and high speed or acceleration is needed [12]. The force characteristics of the VCA is plotted in figure 2.4.

Figure 2.3: The Thorlabs VC125/M VCA used.

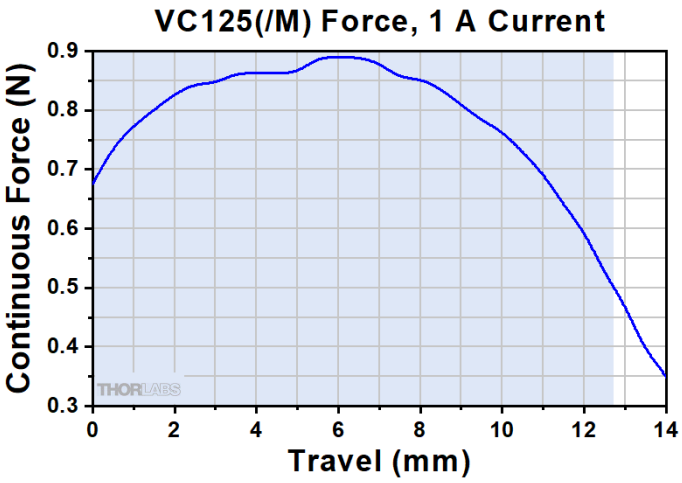

Figure 2.4: Thorlabs VC125/M force characteristics graph [12]

2.2.2 Pulse width modulation

To finely control the actuator, pulse width modulation (PWM) is utilised to vary the effective voltage of a constant source [13]. By rapidly switching the voltage source a square wave will be generated which if integrated has a lower average voltage than the source. Depending on the ratio of time switched on and off the effective voltage can be regulated between 0 % and 100 % of the voltage source. A sine wave and it's corresponding PWM wave is illustrated in figure 2.5.

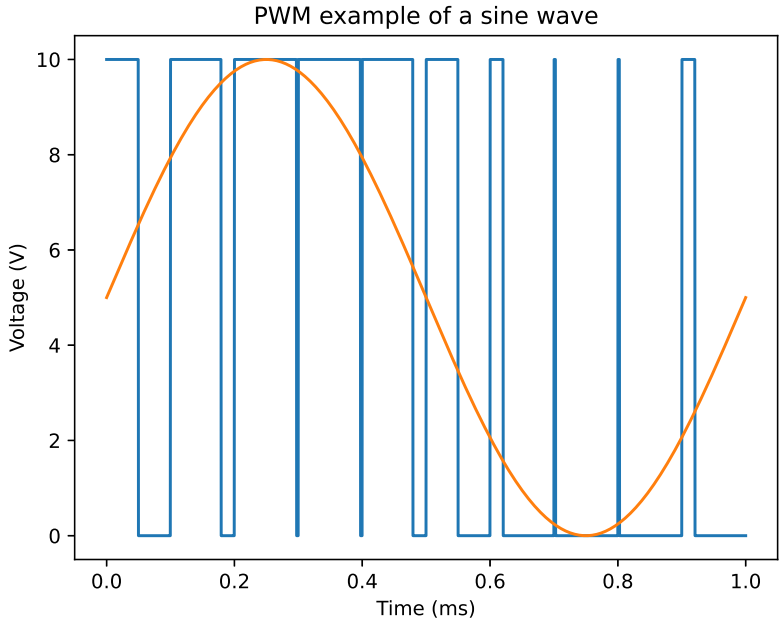

Figure 2.5: A sine wave (orange) converted to a PWN signal (blue).

2.2.3 WEMOS LOLIN32

The WEMOS LOLIN32 (see figure 2.7) is a micro-controller based on the ESP32-WROOM-32 module developed by Espressif [14]. For the scope of this project the PWM capabilities of the controller is of relevance. The ESP32-WROOM-32 has a built in PWM controller with eight high speed and eight low speed channels. With the lower speed (LEDC clock) at 80 MHz. From that information it can be calculated that the clock needs to run at

$$f_{pwm} \cdot 2^{res_{pwm}} \tag{2.2}$$

Hz at least, in order to represent the PWM wave. If the resulting frequency from equation (2.2) $<$ 80 MHz, the desired frequency and resolution can be used.

2.2.4 L298N Dual Full-Bridge Driver

The L298N (see figure 2.6) is a dual channel full-bridge driver [15]. It is capable of driving two DC-motors in both directions, or in the case of a VCA, both extend and contract the actuator. The driver is rated up to 46 V DC with a maximum current output of 4 A split between two channels. The logic of the driver needs a separate 5V supply if driver is operated above 12 V. The driver has a switching delay in the single μs range. The motor driver is controlled via six inputs. ENA and ENB are used to enable the output for channel A and B, if a PWM signal is used the channels will be enabled and disabled accordingly. The remaining four pins control the direction on the motors for the two channels respectively by writing them as HIGH and LOW. The IN1 and IN2 pins control the direction of the motor for channel A. IN3 and IN4 control the direction of the motor for channel B. The two output channels of the L298N can be wired in parallel, to output 4 A as one output.

If the driver is fed with a PWM sine wave to the ENA/ENB pin while the IN1 and IN2 / IN3 and IN4 pins are switched at the correct interval the resulting output wave will be a sine wave. Due to the full bridge behaviour of effectively swapping the polarity, the peak to peak amplitude of the resulting wave will be two times the power supply DC voltage

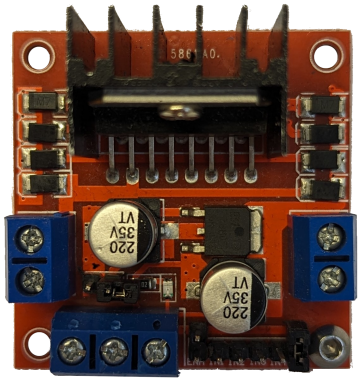

Figure 2.6: The L298N board used

Figure 2.7: The WEMOS LOLIN32 development board used

3
Method

3.1 Prototyping methods

The following section will detail how the iterative development of the design was conducted as well as describe the methods used to manufacture the parts.

3.1.1 CAD

Multiple concepts for the insectoid propulsion system were crafted using CAD, specifically Autodesk Fusion 360 [16], to ensure precision in design and tolerances. Autodesk Fusion 360 enabled simulation of the joinery and dynamic motion of the propulsion system, thereby providing a comprehensive understanding of its functionality and performance before moving on to produce the models.

3.1.2 3D printing

List of materials

1. Ultimaker s3 extended [17] 3D-printer
2. Formlabs Form3+ [18] resin 3D-printer
3. ABS filament
4. PLA filament
5. TPU filament
6. PVA glue
7. Formlabs white v4 resin
8. Formlabs black v4 resin

The g-code for the Ultimaker and Form3 3D-printers were created using the slicer softwares Ultimaker Cura [19] and Preform [20] respectively, with the STL-files exported from the CAD software. In the slicer softwares the print setting could be adjusted to different preferences depending on the material and printing operation.

PLA
The first printed models was printed with PLA-filament because of it's ease of printing. When printing PLA the Ultimaker S3 Extenden [17] was used with Ultimaker Cura [19] recommended settings:

- Layer height: 0.06 mm
- Printing Temperature: 225 °C
- Build Plate Temperature: 60 °C
- Speed: 50 mm/s
- Infill: 20 %
- Cooling: ON
- Support: N/A
- Build Plate Adhesion: Brim

ABS
To improve the stiffness, strength and temperature resistance, the models was printed in ABS. When printing ABS the Ultimaker s3 Extended [17] was used with the Ultimaker Cura [19] recommended settings:

- Layer height: 0.1 mm
- Printing Temperature: 230 °C
- Build Plate Temperature: 80 °C
- Speed: 55 mm/s
- Infill: 20 %
- Cooling: ON
- Support: Tree like
- Build Plate Adhesion: Brim

Resin
For smaller parts, resin-printing with the Form3+ [18] was used to improve the detail quality of the arms and the motor mount. To slice the models Preform [20] was used with default print settings and 0.05 mm layer height as well as its "One-Click print" automatic setup tool.

- Layer height: 0.05 mm
- Print settings: Default

3.1.3 Control system

The control system for adjusting the signal to the voice coil were made up of the following parts:

- L298N Motor driver [15]
- WeMos LOLIN32, ESP32 [14]
- 2x Switches
- Breadboard
- 9x Dupont jumper cables
- Thorlabs VC125/M Voice coil [3]
- 0-15V DC Power Supply

These part were chosen due to ease of access, low cost while being easy to use. The voltage is regulated via the power supply while the frequency is controlled via the ESP32 using PWM. The two switches are wired as inputs to the ESP32 which are used to increase or decrease the delay between steps in the sine look-up table. The code only controls the delay, but as a consequence the delay determines the period which corresponds to a frequency. The ESP32 is programmed in Arduino C++. The components where wired according to figure 3.1, and mounted on a board (figure 3.2.

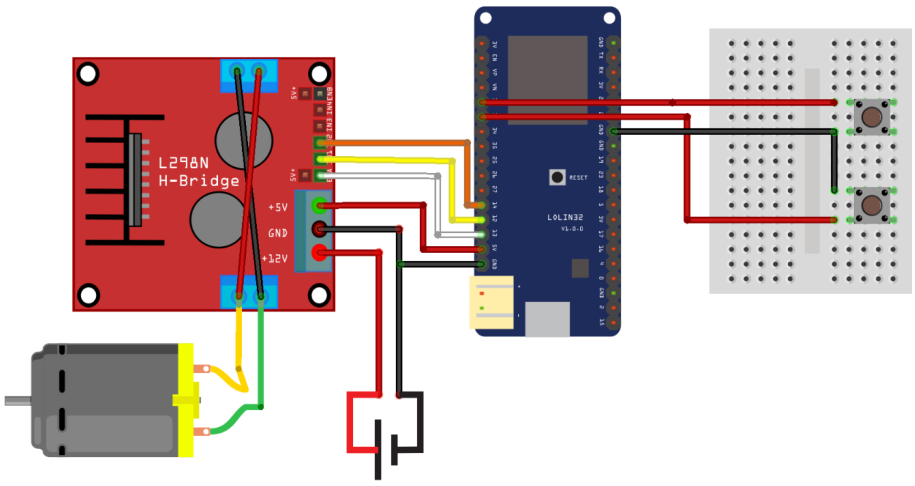

Figure 3.1: Schematic overview showing the wiring of the control board. From the top left: L298N, ESP32, breadboard, motor, DC power supply.

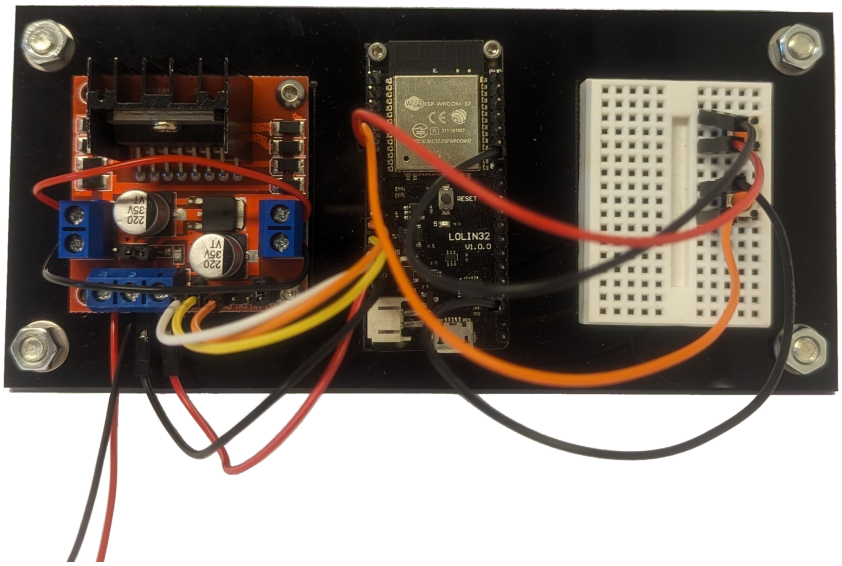

Figure 3.2: The final control board with the different components mounted. From the left: L298N, ESP32, breadboard.

3.1.4 Iterative design process

To design the insectoid propulsion system an iterative design process was used. The process started with the initial planning for different types of designs, these were the compliant, rigid and bistable design. Ideas were tried in CAD as assemblies and then prototypes was made with 3D-printing. The designs were then tried and evaluated. After this, the process started over with the created prototype as a new base model, and the process was repeated. This process was done for the different type of designs at the same time. In the end, only one final design was chosen and used for the final benchmarking. The complete outcomes of the iterated design process is shown under Chapter 4.

3.1.5 Wing designs

Since the performance of the propulsion system is highly linked to the design and layout of the wings and since what is the optimal wing changes depending on multiple factors that will change during the design development. Multiple wing designs were used as to not just find the best transmission design for one particular set of wings, but rather to design a insectoid propulsion system usable in multiple different configurations.

The wing variants was made by scaling a simplified version of the initial prototype wing design. The initial wing design was chosen as a starting point and main reference to avoid evaluating the aerodynamics of the wing. The main focus was directed towards the structure, weight and mechanical rigidity of the wing.

3.1.6 Wing construction

The wing, figure 3.3, is built with a 3d-printed ABS-skeleton, with exception to the top beam which is replaced with a thin carbon fibre rod to increase the stiffness. The "membrane" is constructed of two pieces 0.023 mm mylar film which is heated to ∼200 °C with a Mini iron II [21] which fuses the ABS-skeleton and the mylar film.

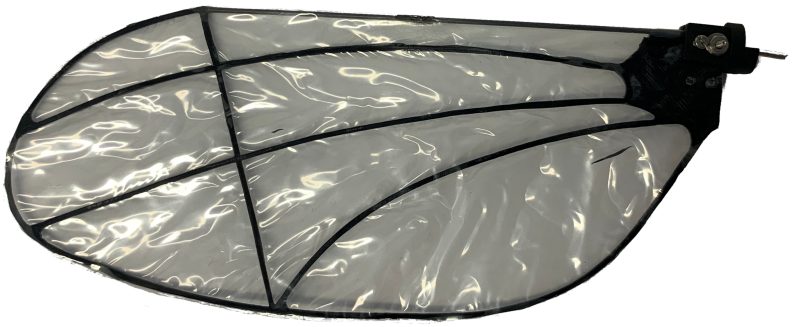

Figure 3.3: Carbon reinforced mylar-wing.

3.2 Characterisation methods

In order to evaluate the final design a method of characterisation was developed. This method enabled data to be gathered and evaluated, to indicate possible further directions of development.

3.2.1 Measuring lift

To determine what combinations of spring and wings produces the most amount of lift, a range of tests were performed on the final design seen in chapter 4 section 4.2. To test the lift and stroke amplitude of the propulsion system it needed to be stationary which prompted for a test rig. A rig was 3D-printed which put the propulsion system in the correct upright position. The rig gave the possibility to mount a spring to the voice coil which was to be tested. The rig's open sides made it easy to remove and mount different wings, which reduced time during testing (see figure 3.4). To measure the lift created from the insectoid propulsion system a Kern 440 [22] scale was used with a precision of ±0.01 g.The rig was then fixed on the scale with double sided adhesion tape which made it possible for the propulsion system to lift the scales plate to recognise generated lift. By zeroing the scale after mounting the rig the measured lift is presented as a negative number on the scales display.

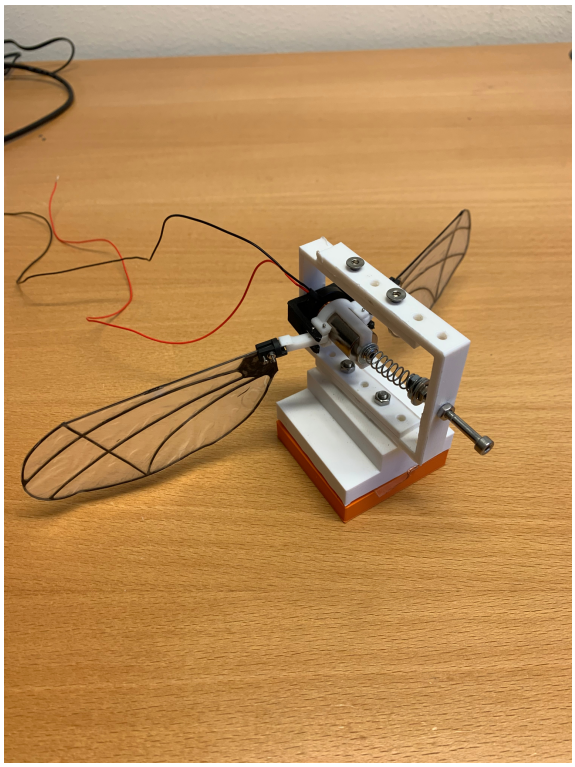

Figure 3.4: Test rig with a spring and the insectoid propulsion system mounted.

3.2.2 Video analysis

To analyse the stroke amplitude and wing beat frequency, a method making use of recorded video and fixed markers where decided on. A camera filmed the propulsion systems's movement from above, see figure 3.5. The camera was zoomed in on only one of the propulsion system's wings, as seen in figure 3.6, to measure the wing movement. The ruler in figure 3.6 is a fixed marker used as a reference to measure the stroke amplitude. The use of a high quality camera provided accuracy of the data analysis. In these test the Sony FX30 cinema line [23] was used with following settings:

- Framerate: 240 fps
- Recording framerate: 24 fps
- Shutter speed: $\frac{1}{8000}$s
- ISO: 20000

The rest of the settings were unchanged.

Figure 3.5: Video setup used to record the wing's stroke amplitude and frequency.

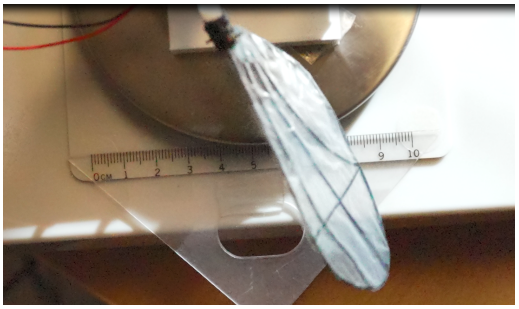

Figure 3.6: View of the wing through the cameras lens.

3.2.3 Wing and spring tests

Test constants:

- 10V from power supply
- 45° angle of attack

Spring constants:

- Soft spring: 64 N/m
- Medium spring: 580 N/m
- Hard spring: 2100 N/m

The entered delays in the code:

- 150 µs
- 200 µs
- 300 µs
- peak µs

Initially, the first of three springs was installed on the rig. The control system of the propulsion system was then adjusted to the minimum delay, and it was operated for a duration of 30 seconds at 10V. This process was subsequently repeated for the remaining delay settings. Following this, the wings were replaced with a different set for further delay testing. Once all five sets of wings had been examined across all delay settings, the spring was switched out, and the entire procedure was carried out once more. This process was performed for each of the three springs, as well as without any spring. During this time, the propulsion system was recorded with the camera and the lift generated was documented in a spreadsheet (see table 4.1). To find the peak lift for a set of wings the delay (frequency) was varied until the most lift was produced. The delay, (Peak delay, 4.1), which corresponded to the maximum lift was documented, along with the maximum lift generated for that set of wings which can be seen in figure 4.1.

3.2.4 Measuring of the stroke amplitude

Logger PRO [24] were used to analyse the video since it offers easy motion tracking by manually adding tracking points to each frame. By placing a known measurement in the frame, a ruler, a reference for scale was set which allows the Logger PRO [24] software to calculate accurate positions of the tracking points in relation to a fixed point. An example of the different tracking points can be seen in figure 3.7. From these position measurements the stroke amplitude were calculated as follows: The Cartesian coordinates from the measurements are converted to polar coordinates, which allows the stroke amplitude to be calculated as in equation 3.1.

$$\theta = \varphi_{max} - \varphi_{min} \tag{3.1}$$

The wingbeat frequency can be calculated through equation 3.2.

$$f_{wing} = \frac{\text{frames per second}}{\text{frames per wingstroke}} \tag{3.2}$$

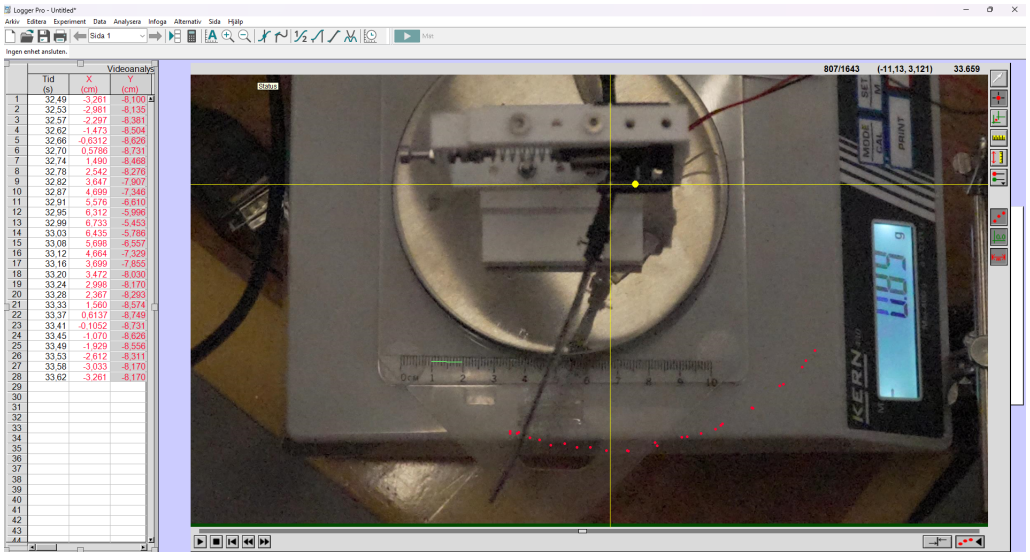

Figure 3.7: Example of measurements in Logger PRO [24].

3.2.5 High voltage test

Once all the necessary data had been gathered, final testing was conducted. Given that the longevity of the VCA was not a concern, the voltage could be increased to 30 V using a different DC power supply. Two promising combinations of wings and springs were selected, and their lift was measured. The motor was operated for a duration of $\sim$ 5 seconds to prevent the plastic from melting or the motor from burning.

4
Results

4.1 Iterative design process concepts

During the iterative design process, a number of concepts were developed and evaluated. Three distinct concepts were explored before a final design was settled on: a compliant design, a bistable design and a rigid design.

4.1.1 Compliant design

The initial prototype of the insectoid propulsion system was of a compliant design of TPU which prompted the continuity of that design. In figure 4.1 there are three models with similar shape and movement characteristics. To the left is the first iteration where the bottom of the body is solid and the upper part bendable to create a transmission. This design had to be printed on its side which made the bendable TPU joints too thick thus absorbing a lot of movement energy. The middle design is the next iteration where the same transmission design was used but the body was printed laying flat like a band. This did need some post-printing rework to make the bottom joints bend correctly. The third model to the right in figure 4.1 was the last iteration which utilised a TPU band. Here the model was printed laying flat with slots where the band needed to bend. This created a transmission with the correct movements, but the TPU absorbed to much energy to make it efficient.

Figure 4.1: Compliant design made of a TPU band.

Another take on the compliant design was to have a rigid body with a transmission made of pliable joints. In figure 4.2 the different iterations of that design are presented. The first design to the left in figure 4.2 used a bendable band of TPU as a transmission to create the wing movements. This design showcased the opportunities with a rigid body compared to to that shown from 4.1. The first model did

however not have enough height for the coil to move correctly. The next iteration heightened the model to fit the coil and shortened the distance of the transmission to increase the stroke amplitude. Despite its design, this model encountered the same issues with the TPU absorbing too much energy when bending. One unique possibility this model had, was the ease of mounting different configuration of the bendable band which made it easier to work with. To minimise the absorption of energy by the TPU and stabilise the movement, a third model was created which had solid arms and mounting plate (the middle part) with flexible material between as joints. This created a design which could give a stroke amplitude of 90° with minimal absorption from bending. The solid parts of the model where printed in ABS for durability and temperature resistance.

Figure 4.2: Compliant design with a rigid body.

4.1.2 Bistable design

A bistable design based on a schematic view of the bistable buckling compliant mechanism in the paper "“Clicking” Compliant Mechanism for Flapping-Wing Micro Aerial Vehicle" by Yao-Wei Chin and Gih-Keong Lau from School of Mechanical and Aerospace Engineering, Nanyang Technological University, Singapore[8] were tested due to showing great promises when trying to maximise the stroke amplitude. However, this idea was discarded after evaluation that led to the realisation of two challenges with this approach. One being that this design would require a very long stroke to work effectively, significantly longer than what the actuator were capable of producing. While it's possible to increase the stroke by connecting the VCA to a stroke amplifier mechanism, this was deemed to be an ineffective solution due to the increased amount of moving parts. The second challenge was the need for the structure to not only be slightly flexible to allow for the mechanism to be bistable but ideally also be an effective spring in order to be able to effectively return the built up energy while bending. This is however not a characteristic of TPU which

instead absorbs a lot of the energy while being bent [25]. Therefore other materials, not accessible in this project, would have to be investigated in order to explore this solution further.

4.1.3 Rigid designs

Due to problems with manufacturing a compliant design, a rigid design was tested to simplify the movement characteristics of the insectoid propulsion system.

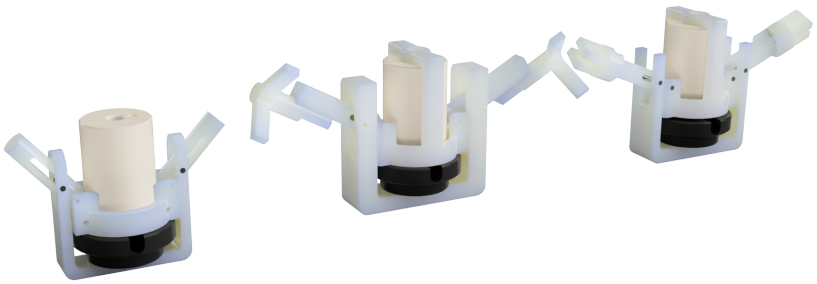

Figure 4.3: Iterations of the rigid transmission design.

The mechanical linkage transmission translates the linear movement of the VCA into the complex oscillating wing movement, thereby generating a wing beat. The VCA base is attached to an u-shaped bracket, while the magnet is attached to the body of the linkage. The arms of the insectoid propulsion system are connected to the body via a pin joint, and the arms themselves are attached to the bracket using pins within a pin-slot configuration The wing mount attaches to the arm via a ball bearing, enabling rotation of the wing throughout the beat. See figure 4.5.

4.2 Final design

During the iterative system design phase, different concepts, parts and configurations were tested. The final design of the insectoid propulsion system is a rigid transmission printed in resin. The propulsion system is mounted on the rig which supports mounting of a spring to the body of the propulsion system. Theoretically this design allows a total stroke amplitude of 94°. To twist the wings, a shaft and ball-bearing is mounted between the arm and the wing holder. The wings has an angle of attack at 45° by having a ledge on the arm and a cut out on the wing holders flange which prevent it from a full turn of the wings, see figure 4.5 for illustration. The final transmission (excluding wings and motor) weigh **3.72** g. The transmission paired with the VCA, as shown in fig 4.4a, comes to a total weight of **21.33** g. The VCA accounts for 82.6% of the transmissions weight.

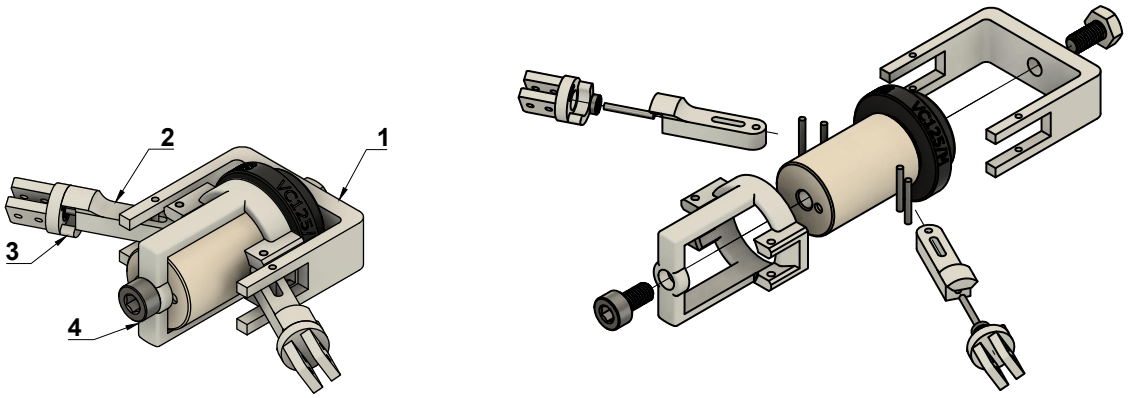

(a) (1) Bracket, (2) Arm, (3) Wing holder, (4) Body

(b) An exploded view

Figure 4.4: Assembled view and exploded view of the final design of the insectoid propulsion system.

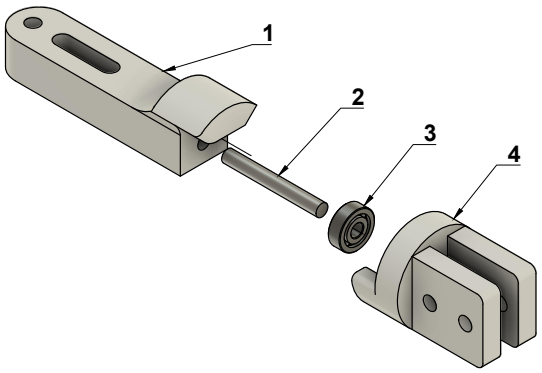

Figure 4.5: A closer view of the arm assembly; (1) Arm, (2) 8 mm stainless steel dowel pin, (3) 3x1x1 ball bearing, (4) Wing holder

4.2.1 Wing material improvements

The use of Mylar for the membrane of the wing resulted in 0.69 g or 48% less weight than the original. During the tests it was discovered that the wings had to be reinforced to be stiffer since the wings tended to self oscillate. The wings were therefore reinforced with carbon fibre rods at the leading edge to increase the stiffness and subsequently reduces the risk of the wing entering self-oscillation.

4.2.2 Wings

The five different wing variants that were created consists of one with the same dimensions as the initial wingdesign at 100x45 mm, or 100% scale, two which were scaled down uniformly lengthwise and widthwise (Thickness was not scaled) 80% and 50% and finally two which were scaled non-uniformly, 120% in one direction and 80% in the other, resulting in one long and thin wing and one short and wide. These wing variants will be referred to as "wing100", "wing80", "wing50", "wing_wide" and "wing_long" respectively. The design is an improved version of the initial wing design. It uses a ABS skeleton with a carbon fibre rod as reinforcement at the leading edge for the scaled versions. A mylar membrane is fused to the skeleton as the surface of the wing, see (figure 4.6).

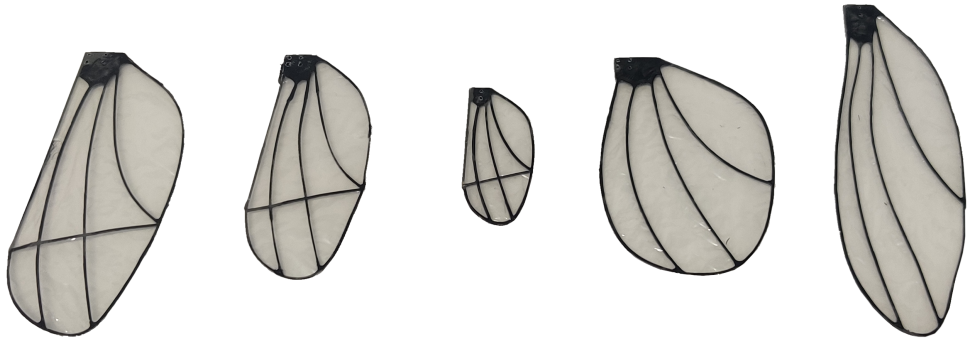

Figure 4.6: All carbon reinforced mylar wings.
From left to right: wing100, wing80, wing50, wing_wide, wing_thin

Weight per set of wings:

- wing50 = 0.43 g
- wing80 = 0.91 g
- wing100 = 1.32 g
- wing_wide = 1.19 g

Projected area for each set of wings:

- wing50 = 1750 mm^2
- wing80 = 5000 mm^2
- wing100 = 7500 mm^2
- wing_wide = 7250 mm^2

4.2.3 Control system

At first, the PWM signal was generated by stepping through a sine-table at varying step lengths, this approach generated problems at high frequencies due to large step sizes. The resulting wave was not sinusoidal in nature due to the limited amount of samples (according to the Nyquist–Shannon sampling theorem) [26]. The result was greatly improved by instead varying a delay between each step in the table, effectively compressing or stretching the wave but keeping the resolution.

The final iteration of the controller uses a pure PWM sine wave, with a PWM frequency at 100 kHz. The PWM output is has a resolution of 8-bits (0-255). The final code for the controller can be seen in appendix A.

4.3 Test results

Table 4.1 shows the result of the tests of different configurations and input signals of the finalised insectoid propulsion system design. The table is divided into four chunks representing test data for the four wings "wing100", "wing80" "wing50" and "wing_wide". The measurements from "wing_long" was excluded due to never producing any observable lift for any configuration or frequency. Within every quadrant the test data is divided into four columns and four rows containing 3 subrows. The columns represent the different springs used in the configuration and four rows representing 3 different delays (which corresponds to the frequency of the input signal), as well as the last one representing the peak values given by fine-adjusting the delay until reaching the maximum lift for each configuration. Within each of these four rows are the 3 subrows showing generated lift in grams of thrust, frequency of the wing flapping in hertz and the stroke amplitude of the wings in degrees. From the raw data in this table a pair of plots, figure 4.7 and figure 4.8, were created from which some interesting results can be observed. From the tracking data measured in Logger PRO [24] radial graphs visualising the stroke amplitude of the wings could be generated, see figure 4.9.

In figure 4.7, the lift is plotted as size and colour in relation to the spring and wing configuration. From the figure it can be observed that the most lift were generated by the larger wing80 and wing100 using a soft spring. While the soft spring resulted in the most lift for these wings the somewhat stiffer spring were more suitable for the smallest of the wings while the wide wing worked the best without any spring attached.

The data also resulted in the plot in figure 4.8 plotting the measured lift on the y-axis in correlation to the frequency of the wings on the x-axis with different lines representing different configurations. A clear trend between frequency and the produced lift can be seen in the figure. Most noticeable is the clear overall downward trend in the data clearly showing that wing80 and wing100 both with soft springs generated the most lift of all at 1.39 g and 1.3 g of thrust and at the low frequencies of 8 Hz and 5 Hz respectively. Upon closer observations of the plot other interesting trends emerge. While many of the individual configurations show a downward trend, it is however noteworthy to point out that the wing50 with the hard spring shows a clear increasing trend between frequency and lift. The observed trend of lift and frequency for the different wings is the same when looking at all the data. The difference is most striking when comparing the two extremes, wing50 with a hard spring and wing100 with a soft spring, see figure 4.8.

The final test at 30 V resulted in a maximum lift of 4.03 g with medium spring combined with wing80, the medium spring with the wing100 resulted in 3.45 g lift.

Table 4.1: Table of the raw data observed from the testing. Values marked "–" signifies that no measurable lift was produced for that combination. All measurements at 10 V.

		Wing 50%				Wing 80%			
Delay (μ s)	measures	no spring	Spring soft	Spring Medium	Spring Hard	no spring	Spring soft	Spring Medium	Spring Hard
150	Lift (g)	0.17	0.19	0.1	0.41	–	0.13	–	–
150	Frequency (Hz)	24	21.8	24	21.8	–	–	–	–
150	Stroke amplitude (degree)	4.3	19.9	34.6	31.33	–	–	–	–
200	Lift (g)	0.29	0.45	0.65	0.3	–	0,1 - 0,3	–	–
200	Freq	18.5	17.1	17.1	18.5	–	17.1	–	–
200	Stroke amplitude (degree)	24.6	72.1	69	41.5	–	23.6	–	–
300	Lift (g)	0.7	0.52	0.44	0.05	0.37	0.49	0.3	0.32
300	Frequency (Hz)	12	12.6	12.6	12.6	12	13.3	12.6	12
300	Stroke amplitude (degree)	95.1	83.9	78.7	24.7	16.5	23	40.4	30.2
Peak	Lift (g)	0.72	0.6	0.85	0.52	0.7	1.39	0.93	0.4
Peak	Frequency (Hz)	13.3	12.6	15	21.8	8.3	8	8.9	12
Peak	Stroke amplitude (degree)	84.3	82	62.9	37.8	69	85.5	71.2	33
Peak delay	Delay (\mu s)	–	270	220	165	–	495	425	300
		Wing 100%				Wing Wide			
		No spring	Spring soft	Spring Medium	Spring Hard	No spring	Spring soft	Spring Medium	Spring Hard
150	Lift (g)	–	–	–	–	–	–	–	–
150	Frequency (Hz)	–	–	–	–	–	–	–	–
150	Stroke amplitude (degree)	–	–	–	–	–	–	–	–
200	Lift (g)	–	–	–	–	–	–	–	–
200	Freq	–	–	–	–	–	–	–	–
200	Stroke amplitude (degree)	–	–	–	–	–	–	–	–
300	Lift (g)	0.5	0,2 - 0,4	–	–	–	–	–	–
300	Frequency (Hz)	12	13.3	–	–	–	–	–	–
300	Stroke amplitude (degree)	15.1	18	–	–	–	–	–	–
Peak	Lift (g)	0.5	1.3	0.39	–	0.9	0.8	0.5	–
Peak	Frequency (Hz)	12	4.9	12	–	8	7.1	8.9	–
Peak	Stroke amplitude (degree)	15.1	85	29.2	–	49.1	55.9	59.8	–
Peak delay	Delay (\mu s)	300	795	870	–	500	500	435	–

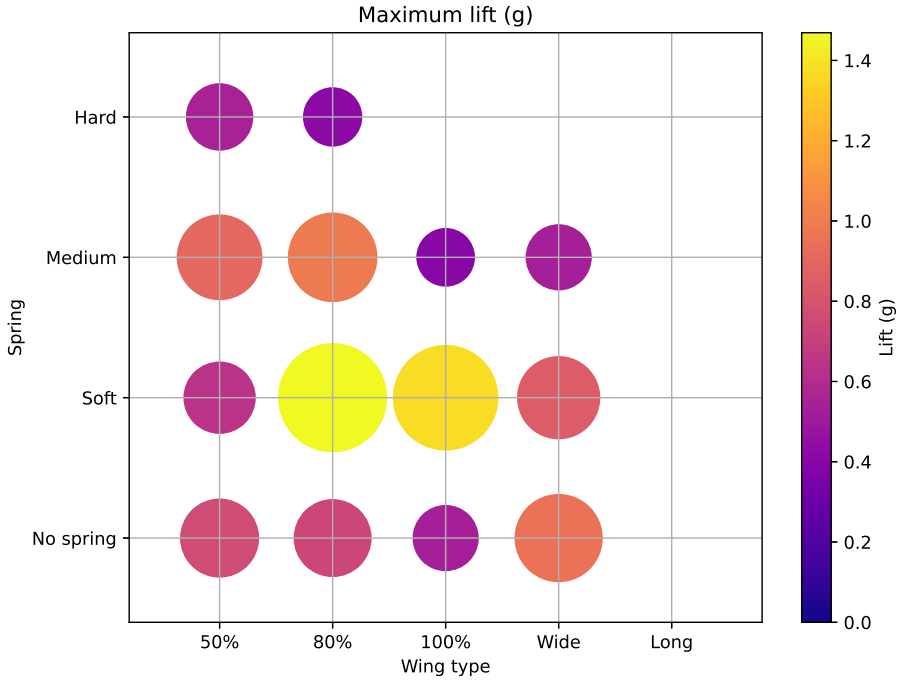

Figure 4.7: The measured maximum lift for each pair of springs and wings.

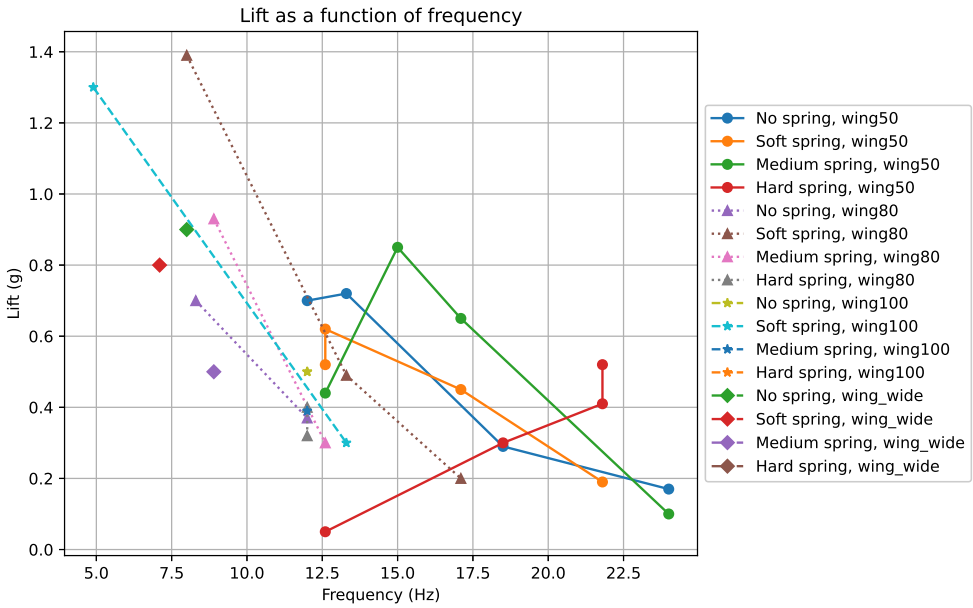

Figure 4.8: Lift generated by the different wings and springs at different frequencies.

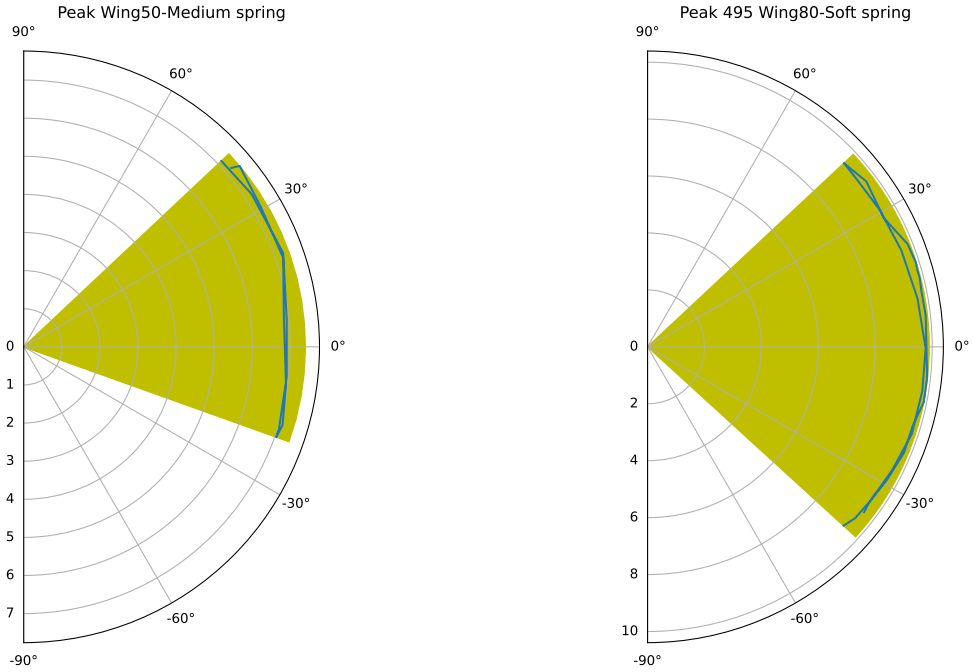

(a) Wing50 with a medium spring.

(b) Wing80 with a soft spring.

Figure 4.9: The measured stroke amplitude for two combinations, at peak lift. The green area is the stroke amplitude, while the blue line is the path of the wing during the stroke.

5
Discussion & Conclusion

5.1 Conclusions from tests

The objective of the project was to design a propulsion system that mimicked the way insects generate lift and propulsion through flapping their wings. The results show that the constructed propulsion system generate lift for a variety of wings and oscillation configurations. The maximum lift generated at 10V was in the configuration shown in table 5.1.

Wing	**Frequency**	**Spring**	**Lift**
Wing80	8 Hz	Soft	1.39 g

Table 5.1: The configuration for the maximum lift generated at 10 V.

The 1.39 g of produced lift was not enough for takeoff as the complete propulsion systems weight in the configuration was **22.24** g. The generated lift accounted for 6.24% of the necessary lift for takeoff. Even Though the number may seem small, this is still considered a great improvement as the lift generated is stable and a vast difference compared to the base models propulsion system which had ∼0 g generated lift and a total weight of 44.81 g. The propulsion system has halved in weight and improved to 1.39 g of lift. With the 30V test, a conclusion can be drawn that the lift generated is primarily restricted by the motor. With an increase to 4.03 g lift at 30 V, the body's design is proven to be well suited for generating more lift if the power of the motor could be increased.

Before tests, the efficiency of the wing's kinematics was hypothesised to be partially influenced by the natural frequency of the wing around the pitch axes. This natural frequency is prompted by gravitational forces which treats the wing as a pendulum. While it may not be optimal to resonate the wing in pitch, the optimal frequency is assumed to scale to the the wing's natural frequency. Furthermore, the natural frequency of a pendulum is inversely proportional to its length, this implies that larger wings should be optimal at lower frequencies and vice-versa. This also hypothesise that larger wings are expected to generate higher lift when paired with less stiff springs. The test results support this hypothesis. As seen in table 4.1, a wing at its full length (100%) is observed to be optimal without a spring, an 80% wing is optimal with a soft spring, and a 50% wing is optimal with a medium spring. For further development, this relation should be taken into account when deciding which spring or wings to choose.

5.2 Design features

During the design process a number of different designs based on concepts found in scientific literature, or developed during the design process, were tested. These led to insights that wasn't obvious at first sight. The following section describes the different concepts explored during the project.

5.2.1 Compliant transmission

While the compliant joints of the transmission had great potential regarding being compact and simple as well as low resistance to movement, its main downfall in this project were due to manufacturing difficulties. The TPU used performed well in the thinner sections, serving as flexible joints due to their minimal thickness. This allowed them to bend with low resistance. Provided they were kept short, the joint's movement was limited to bending with a tiny radius and virtually no room for deviation. This resulted in the joints mimicking the behaviour of a hinge quite closely. The TPU did however not work well in the thicker sections as rigid arms as they were still quite flexible. Using dual printing methods to combine the flexible TPU in the thin flexible sections and using the more rigid filament like PLA or ABS for the thicker rigid arms still has great potential but due to difficulties with the dual printers available in this project and time constraints this development had to be abandoned.

As the insectoid propulsion system demands a light body, a compliant mechanism is the best option. With a compliant mechanism, wear would be minimised on the parts which leads to a better longevity of the propulsion system. A compliant design would most likely make a simpler design where fewer body parts could be utilised and assembly would be simpler. The problem that has to be dealt with if a compliant mechanism is to be designed is foremost the combination of material properties for the compliant joints and manufacturing of said joints. At the compliant joints, a thin, strong, wear resistant and pliable material would be optimal. This material could be used for short distances, to minimise buckling and gearing ratio, between the rigid mounting points as seen on the last iteration of a compliant transmission in figure 4.2.

5.2.2 Rigid design

The final design used was a rigid design which accomplished the propulsion system to generate lift. Even though the purpose was accomplished, the designs advantages and disadvantages are presented here. In the rigid design, positioning the axis of rotation of the arms in close proximity to the body allows for a larger stroke amplitude while the VCA can be operated with a low amplitude. Compared to the compliant design, the rigid transmission simplifies complex relations in the movements. The introduction of pin-joints with rotating or sliding surfaces does increase the friction of the design which results in the joints having problems with excessive wear. This could be mitigated by incorporating wear resistant and friction reducing bushings or

bearings, although that would increase the manufacturing complexity and weight. By the nature of the rigid design, there was play in the model. This was necessary to have so the arms could turn and move. The problem with the play was that it sometimes lead to undesirable movements when the model was in oscillation. The propulsion system could sometimes also lock up against one side, like a drawer does which prompted a larger movement of one wing than the other. The play increased with the use of the parts over time which lead to recurring replacement of the parts. If a rigid transmission is to be further developed, the primary objective would be to improve tolerances and reduce wear in the joints. The main problem with the rigid transmission is that the joints wear out fast which quickly reduces the effecitveness of the design. By adding something like a small bronze bushing in the rotational joints the tolerance and wear resistance could be improved substantially, however this would increase complexity and manufacturing time. The pin slot design in the arms could be lined with a low friction self lubricating material like PTFE to reduce friction. The design could utilise bearings to reduce friction and improve tolerances, however the spacial and manufacturing constraints make this hard, which is why the initial bearing design was abandoned. Bearings also increase the weight, but not by an amount which prompts for abandoning the concept as a whole.

5.2.3 Manufacturing method

By constructing the insectoid propulsion system with 3D-printing in the small scale wanted, a lot of problems with 3D-printing as a manufacturing method occurred. When using FDM, the extruded filament width is limited by the nozzle size. In the case of the propulsion systems construction, the FDM-printers at hand had a minimum nozzle size of 0.4mm which was too large for the body-parts. SLA-printing did improve the detail of the body parts but could not deliver the same strength as FDM-printed ABS.

5.3 Electronics

The electronics used in this project were chosen mainly due to their low cost, ease of use and availability. The following section discusses some of the advantages and disadvantages of the current components used in the final design.

5.3.1 Motor

Although the motor was not changed in this project to keep it within the boundaries, it should be noted that the current motor, (VCA), does not produce enough power, as is. If flight and integration of the control system is to be achieved, a motor with higher power-to-weight ratio is required. If the propulsion system is to be powered by something like a common 3.7 V drone battery (with a reasonable weight), a motor which could deliver significantly higher power at a lower voltage would be needed. With the current configuration it does not seem feasible to achieve integrated liftoff with the current motor.

5.3.2 Motor driver

The L298N is based on very old BJT transistor technology which results in a (relatively) large voltage drop of $\sim 1.4\,\mathrm{V}$ over the motor driver. With a current of $2\,\mathrm{A}$ the driver would need to dissipate $2.8\,\mathrm{W}$ of heat, as a result power is wasted and the driver runs hot. This inefficiency necessitates a rather large heat sink for the motor driver, which is heavy. Further, due to the old technology the resulting PWM wave is noisy. If the motor driver were to be mounted to the insectoid propulsion system, the current L298N driver would be too heavy, too hot and too noisy.

With the limitation of the L298N in mind it would probably be wise to investigate new MOSFET based motor drivers. These driver are both small in size and lighter, but also have almost no voltage drop over the driver. As a result of the low voltage drop, the resulting heat is lowered substantially, however a heat sink could still be required depending on which driver is used. In order to not be limited by the motor driver, the new driver would benefit from being able to operate at $24\,\mathrm{V}$, $4\,\mathrm{A}$ or preferably higher. A driver based on something like the *AOD4184A* MOSFET, or similar designs, could be interesting to investigate further.

5.3.3 Control unit

The ESP32-WROOM32 based WEMOS LOLIN32 is a development board which is suited for experimental circuits and wide use cases such as in this project. The propulsion system requires a relatively fast processor in order to step through the sine-table fast enough, to be able to accomplish 10-30 Hz. For this reason the ESP32 (max 240 MHz clock speed) is better suited compared to an Arduino (atmega328p, max 20 MHz) to generate the PWM signal. If a ESP32 is to be mounted on the propulsion system, the smallest development board possible should be used. Since a lot of the circuitry on a development board is not needed for the projects specific use case, if weight is to be fully minimised, a custom PCB with a ESP32 module combined with an external UART programming board would be required. A completely different control unit could also be of interest, since the ESP32 was chosen mainly due to ease of programming combined with the modules high performance.

5.4 Experimental accuracy

The method of measuring used in this project was relatively novel in order to preserve time, but at large the data was usable and accurate enough to draw conclusion. It should however be noted that the measurements could be improved which the following section briefly discusses.

5.4.1 Logger PRO

An aspect to take into consideration when discussing accuracies in the tests with Logger PRO [24] is that in some video clips, the axle (which the origin was positioned at), were out of frame. This was corrected by setting the fixed point as close to the axle as possible and adjusting this the data afterwards with a value decided on by measuring the distance from the fixed point to the axle on the actual model.

5.4.2 Stroke amplitude & frequency

When calculating the stroke amplitude and frequency there is an inaccuracy to consider due to the frame rate which the tests were filmed in. The inaccuracy occurs at the end of the wing stroke when the wing switches direction and the camera doesn't capture the exact end position of the wing. This inaccuracy however is negligible since it doesn't cause significant disturbances.

5.4.3 Measuring lift

As a result of the low placement of the propulsion system on the test rig close to the surface of the scale's plate and the surface of the table it is not improbable that aspects such as ground effect [27] and the fact that parts of the air being pushed downward would push down on the scale, resulting in some lift force measuring being cancelled out, slightly affecting the reading of the scale. While probably not in significant amounts it might be noticeable compared to the amount of lift generation.

An alternative is to keep measuring lift with the scale by relocating the propulsion system in order to reduce interference with turbulent air, see figure 5.1a. It could be interesting to look at a more refined test rig to measure lift. The most reasonable alternative is probably to use a load cell (suited for sub gram precision and rated for at least 70 g) and logging the readouts digitally. The load cell, if mounted correctly, wouldn't be effected by turbulence at all. See figure 5.1b.

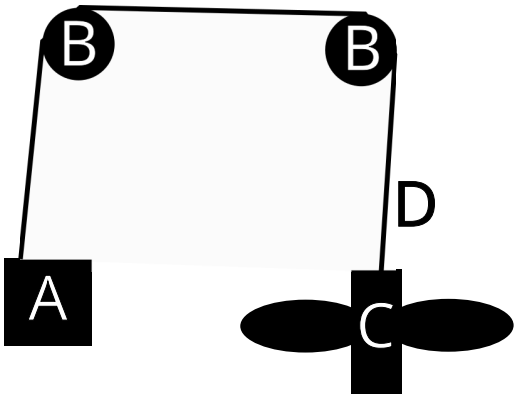

(a) The insectoid propulsion system mounted away from the scale to reduce turbulence.
(A) Scale, (B) bearings, (C) insectoid propulsion system, (D) Cable

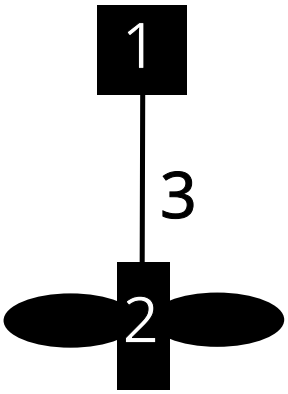

(b) The propulsion system mounted hanging by a load cell.
(1) Load cell, (2) propulsion system, (3) mounting rod

Figure 5.1: Two examples of how the test accuracy could be improved.

Bibliography

[1] E. Farrell Helbling and Robert J. Wood. "A Review of Propulsion, Power, and Control Architectures for Insect-Scale Flapping-Wing Vehicles". In: *Applied Mechanics Reviews* 70.1 (Jan. 2018), p. 010801. ISSN: 0003-6900. DOI: 10.1115/1.4038795.

[2] Noah Jafferis et al. "Untethered flight of an insect-sized flapping-wing microscale aerial vehicle". In: *Nature* 570 (June 2019), pp. 491–495. DOI: 10.1038/s41586-019-1322-0.

[3] *12.7 mm Travel Voice Coil Actuator, SM05 External Thread, Metric*. TTN215763-S01. Rev B. Thorlabs. Sept. 2023.

[4] Michael Dickinson. "Insect flight". In: *Current Biology* 16.9 (2006), R309–R314. ISSN: 0960-9822. DOI: https://doi.org/10.1016/j.cub.2006.03.087.

[5] Larry L. Howell. "Compliant Mechanisms". In: *21st Century Kinematics*. Ed. by J. Michael McCarthy. London: Springer London, 2013, pp. 189–216. ISBN: 978-1-4471-4510-3.

[6] Lindsey Hines, Domenico Campolo, and Metin Sitti. "Liftoff of a Motor-Driven, Flapping-Wing Microaerial Vehicle Capable of Resonance". In: *IEEE Transactions on Robotics* 30.1 (2014), pp. 220–232. DOI: 10.1109/TRO.2013.2280057.

[7] Anaxibia. *Scheme of insect wing movement*. [Last accessed May 7, 2024]. 2024. URL: https://commons.wikimedia.org/wiki/user:Anaxibia.

[8] Yao-Wei Chin and Gih-Keong Lau. ""Clicking" compliant mechanism for flapping-wing micro aerial vehicle". In: *2012 IEEE/RSJ International Conference on Intelligent Robots and Systems*. 2012, pp. 126–131. DOI: 10.1109/IROS.2012.6385809.

[9] Bin Tang and M.J. Brennan. "On the dynamic behaviour of the "click" mechanism in dipteran flight". In: *Journal of Theoretical Biology* 289 (2011), pp. 173–180. ISSN: 0022-5193. DOI: https://doi.org/10.1016/j.jtbi.2011.08.039.

[10] Moticont. *Linear Voice Coil Motors*. Last accessed 5 March 2024.

[11] Today's Medical Developments. *Understanding the basics of a voice coil actuator*. Last accessed 5 March 2024. URL: https://www.todaysmedicaldevelopments.com/article/understanding-the-basics-of-a-voice-coil-actuator/.

[12] Thorlabs. *Voice Coil Actuators*. Last accessed 5 March 2024. URL: https://www.thorlabs.com/newgrouppage9.cfm?objectgroup_id=14116.

[13] J. Szymanski A. Butterfield. *A dictionary of electronics and electrical engineering*. en. Oxford University Press, 2018.
[14] *ESP32 Technical Reference Manual*. ESP32. Version 5.1. Espressif Systems. Apr. 2024.
[15] *L298N Datasheet Dual full-bridge driver*. L298N. Rev 5. STMicroelectronics. Oct. 2023.
[16] Autodesk. *Fusion 360*. Version 2.0.18719 x86_64. 2024. URL: https://www.autodesk.se/products/fusion-360/overview.
[17] Ultimaker. *S3 extended*. URL: https://formlabs.com/eu/software/preform/.
[18] Formlabs. *Form3+*. Version Form3+. 2022. URL: https://formlabs.com/eu/3d-printers/form-3/.
[19] Ultimaker. *Ultimaker Cura*. Version 5.6.0. 2024. URL: https://ultimaker.com/software/ultimaker-cura/.
[20] Formlabs. *Preform*. Version 3.33.3. 2024. URL: https://formlabs.com/eu/software/preform/.
[21] LTD Clover MFG. CO. *Mini Iron II "The adapter"*. Version 5.6.0. 2024. URL: https://www.clover-mfg.com/en/product/n8003eu/.
[22] Kern & Sohn. *Kern 440-35N*. Version Kern 440-35N. 2024. URL: https://www.kern-sohn.com/cosmoshop/default/pix/a/media/440-35N/SL_440-35N_en.pdf.
[23] Sony. *FX30 Cinema Line*. Version FX30 cinemaline. 2023. URL: https://www.sony.co.uk/interchangeable-lens-cameras/products/ilme-fx30.
[24] Vernier. *Logger Pro 3.16.2 Swedish*. Version 3.16.2 Swedish. 2019. URL: https://www.vernier.com/product/logger-pro-3/.
[25] Nava Khatri and Paul Egan. "Energy Absorption of 3D Printed ABS and TPU Multimaterial Honeycomb Structures". In: *3D Printing and Additive Manufacturing* 11 (Feb. 2023). DOI: 10.1089/3dp.2022.0196.
[26] Marcel Escudier and Tony Atkins. *Nyquist–Shannon sampling theorem*. 2019. DOI: 10.1093/acref/9780198832102.013.4218.
[27] J. Wu and N. Zhao. "Ground Effect on Flapping Wing". In: *Procedia Engineering* 67 (2013). 7th Asian-Pacific Conference on Aerospace Technology and Science, 7th APCATS 2013, pp. 295–302. ISSN: 1877-7058. DOI: https://doi.org/10.1016/j.proeng.2013.12.029. URL: https://www.sciencedirect.com/science/article/pii/S1877705813018626.

A

Control system code

```
#define IN1 12
#define IN2 14
#define ENA 13
#define BUTTON_PIN_1 33
#define BUTTON_PIN_2 32

volatile bool buttonPressed1 = false;
volatile bool buttonPressed2 = false;

int timer = 250; // Initial timer value

unsigned char sinetable[256]={
  128, 131, 134, 137, 140, 144, 147, 150, 153,
  156, 159, 162, 165, 168, 171, 174, 177, 179, 182, 185, 188, 191,
  ↪  193, 196,
  199, 201, 204, 206, 209, 211, 213, 216, 218, 220, 222, 224, 226,
  ↪  228, 230,
  232, 234, 235, 237, 239, 240, 241, 243, 244, 245, 246, 248, 249,
  ↪  250, 250,
  251, 252, 253, 253, 254, 254, 254, 255, 255, 255, 255, 255, 255,
  ↪  255, 254,
  254, 254, 253, 253, 252, 251, 250, 250, 249, 248, 246, 245, 244,
  ↪  243, 241,
  240, 239, 237, 235, 234, 232, 230, 228, 226, 224, 222, 220, 218,
  ↪  216, 213,
  211, 209, 206, 204, 201, 199, 196, 193, 191, 188, 185, 182, 179,
  ↪  177, 174,
  171, 168, 165, 162, 159, 156, 153, 150, 147, 144, 140, 137, 134,
  ↪  131, 128,
  125, 122, 119, 116, 112, 109, 106, 103, 100, 97, 94, 91, 88, 85,
  ↪  82, 79, 77,
  74, 71, 68, 65, 63, 60, 57, 55, 52, 50, 47, 45, 43, 40, 38, 36, 34,
  ↪  32, 30,
  28, 26, 24, 22, 21, 19, 17, 16, 15, 13, 12, 11, 10, 8, 7, 6, 6, 5,
  ↪  4, 3, 3,
  2, 2, 2, 1, 1, 1, 1, 1, 1, 1, 2, 2, 2, 3, 3, 4, 5, 6, 6, 7, 8, 10,
  ↪  11, 12,
```

```
  13, 15, 16, 17, 19, 21, 22, 24, 26, 28, 30, 32, 34, 36, 38, 40, 43,
  ↪ 45, 47,
  50, 52, 55, 57, 60, 63, 65, 68, 71, 74, 77, 79, 82, 85, 88, 91, 94,
  ↪ 97, 100,
  103, 106, 109, 112, 116, 119, 122, 125
};

// PWM settings
const int PWM_CH = 0; // ESP32 pwm channel 0-15
const int PWM_FREQ = 100000; // PWM Freq. Keep over human hearing
↪ freq to avoid noise
const int PWM_RES = 8; // 8 bits, 0-255, ESP32 max 16 bits
int value;
unsigned char u = 0;
unsigned char *p = sinetable;

void IRAM_ATTR button1ISR() {
  buttonPressed1 = true;
}

void IRAM_ATTR button2ISR() {
  buttonPressed2 = true;
}

void setup() {
  pinMode(ENA, OUTPUT);
  pinMode(IN1, OUTPUT);
  pinMode(IN2, OUTPUT);
  pinMode(BUTTON_PIN_1, INPUT_PULLUP);
  pinMode(BUTTON_PIN_2, INPUT_PULLUP);
  attachInterrupt(digitalPinToInterrupt(BUTTON_PIN_1), button1ISR,
  ↪ FALLING);
  attachInterrupt(digitalPinToInterrupt(BUTTON_PIN_2), button2ISR,
  ↪ FALLING);
  Serial.begin(9600); // Adjust baud rate as necessary
  ledcSetup(PWM_CH, PWM_FREQ, PWM_RES);
  ledcAttachPin(ENA, PWM_CH);
}

void loop() {
  if (buttonPressed1) {
    buttonPressed1 = false;
    // Increase timer value by 5 steps
    timer = min(timer + 5, 1000); // Limit to maximum value
  }
```

```
  if (buttonPressed2) {
    buttonPressed2 = false;
    // Decrease timer value by 5 steps
    timer = max(timer - 5, 0); // Limit to minimum value
  }

  value = p[u++];

  digitalWrite(IN1, (value > 127) ? HIGH : LOW);
  digitalWrite(IN2, (value > 127) ? LOW : HIGH);
  ledcWrite(PWM_CH, abs(2 * (value - 127)));
  delayMicroseconds(timer);
}
```

B

Stroke plane from tests

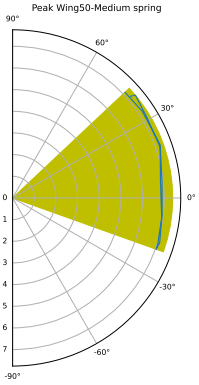
Peak Wing50-Medium spring

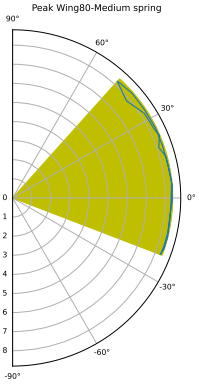
Peak Wing80-Medium spring

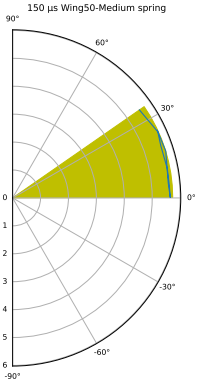
150 µs Wing50-Medium spring

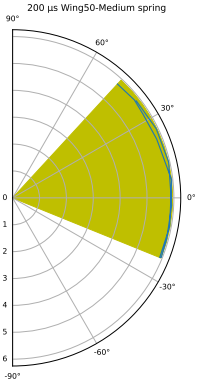
200 µs Wing50-Medium spring

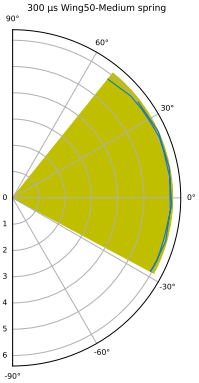
300 µs Wing50-Medium spring

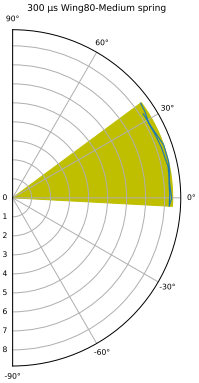
300 µs Wing80-Medium spring

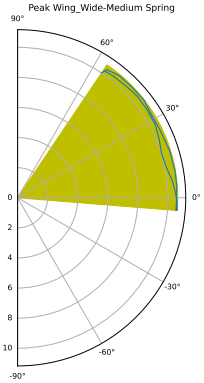
Peak Wing_Wide-Medium Spring

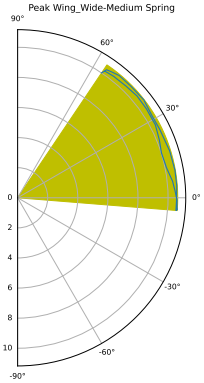
Peak Wing_Wide-Medium Spring

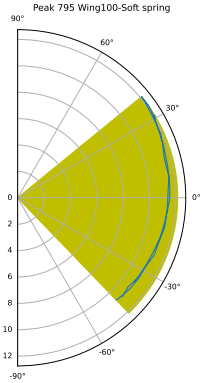
Peak 795 Wing100-Soft spring

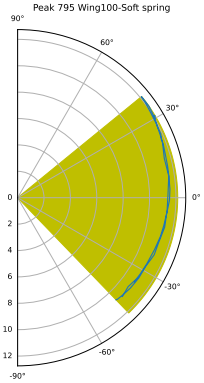
Peak 795 Wing100-Soft spring

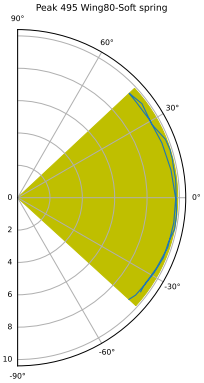
Peak 495 Wing80-Soft spring

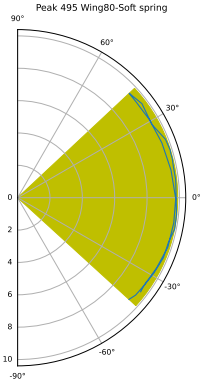
Peak 495 Wing80-Soft spring

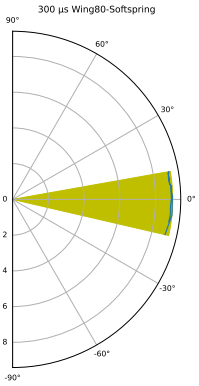
300 µs Wing80-Softspring
90°
60°
30°
0°
-30°
-60°
-90°

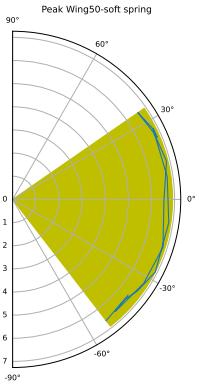
Peak Wing50-soft spring
90°
60°
30°
0°
-30°
-60°
-90°

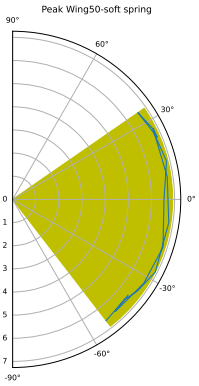
Peak Wing50-soft spring
90°
60°
30°
0°
-30°
-60°
-90°

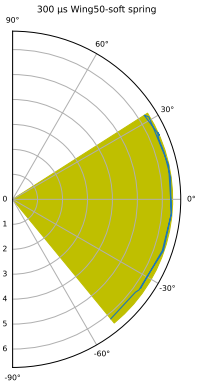
300 µs Wing50-soft spring
90°
60°
30°
0°
-30°
-60°
-90°

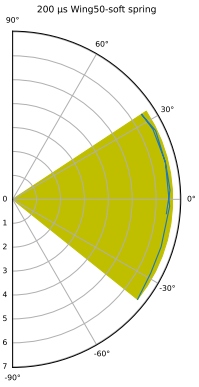
200 µs Wing50-soft spring
90°
60°
30°
0°
-30°
-60°
-90°

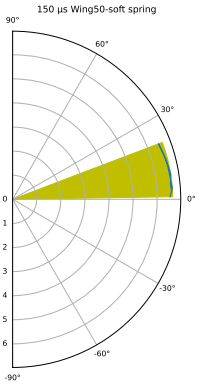
150 µs Wing50-soft spring
90°
60°
30°
0°
-30°
-60°
-90°

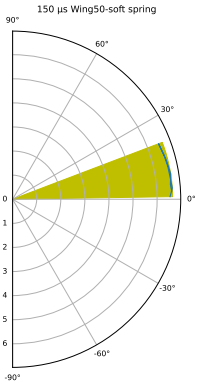
150 µs Wing50-soft spring
90°
60°
30°
0°
-30°
-60°
-90°

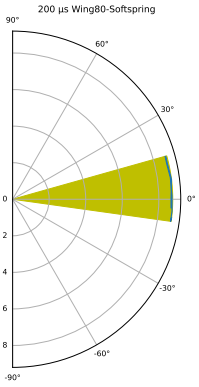
200 µs Wing80-Softspring
90°
60°
30°
0°
-30°
-60°
-90°

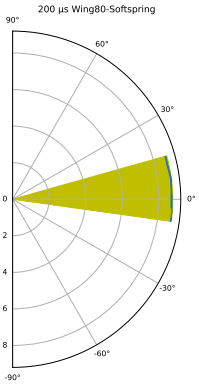
200 µs Wing80-Softspring
90°
60°
30°
0°
-30°
-60°
-90°

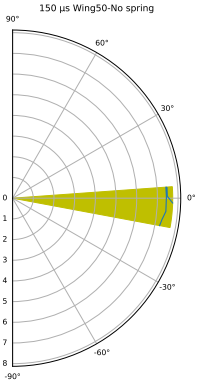
150 µs Wing50-No spring
90°
60°
30°
0°
-30°
-60°
-90°

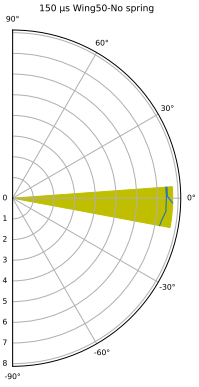
150 µs Wing50-No spring
90°
60°
30°
0°
-30°
-60°
-90°

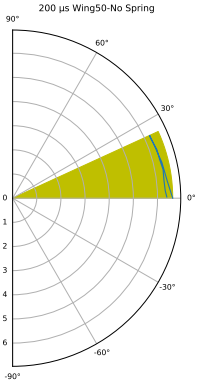
200 µs Wing50-No Spring
90°
60°
30°
0°
-30°
-60°
-90°

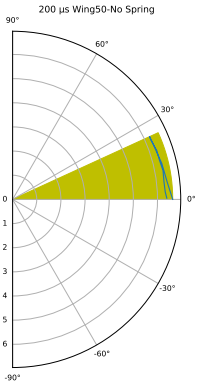
200 µs Wing50-No Spring
90°
60°
30°
0°
-30°
-60°
-90°

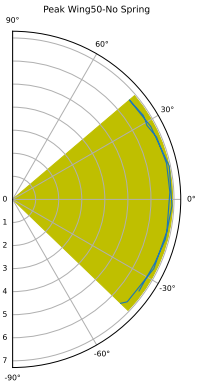
Peak Wing50-No Spring
90°
60°
30°
0°
-30°
-60°
-90°

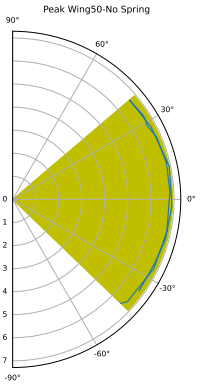
Peak Wing50-No Spring
90°
60°
30°
0°
-30°
-60°
-90°

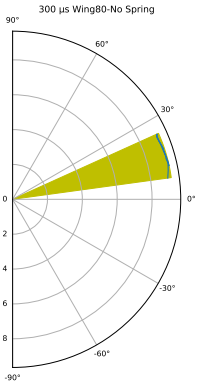
300 µs Wing80-No Spring
90°
60°
30°
0°
-30°
-60°
-90°

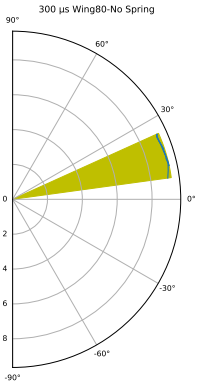
300 µs Wing80-No Spring
90°
60°
30°
0°
-30°
-60°
-90°

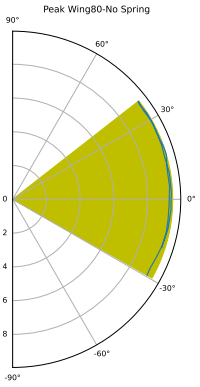
Peak Wing80-No Spring
90°
60°
30°
0°
-30°
-60°
-90°

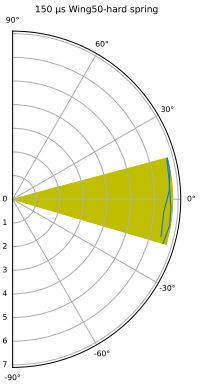
150 µs Wing50-hard spring
90°
60°
30°
0°
-30°
-60°
-90°

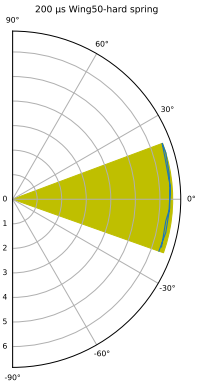
200 µs Wing50-hard spring
90°
60°
30°
0°
-30°
-60°
-90°

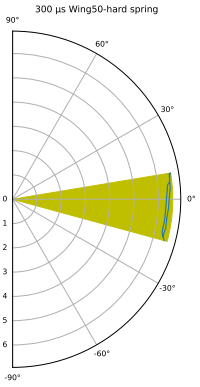
300 µs Wing50-hard spring
90°
60°
30°
0°
-30°
-60°
-90°

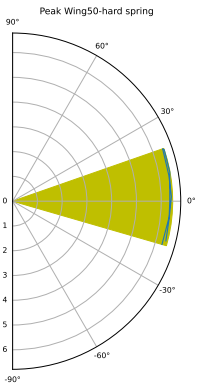
Peak Wing50-hard spring
90°
60°
30°
0°
-30°
-60°
-90°

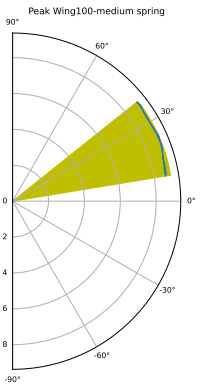
Peak Wing100-medium spring
90°
60°
30°
0°
-30°
-60°
-90°

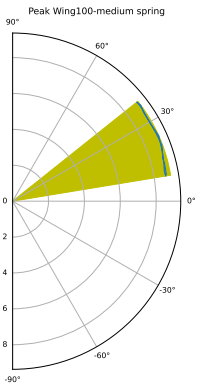
Peak Wing100-medium spring
90°
60°
30°
0°
-30°
-60°
-90°

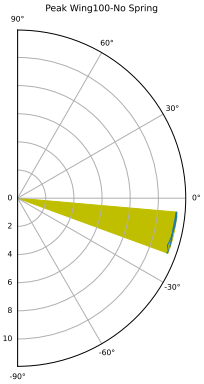
Peak Wing100-No Spring
90°
60°
30°
0°
-30°
-60°
-90°
0
2
4
6
8
10

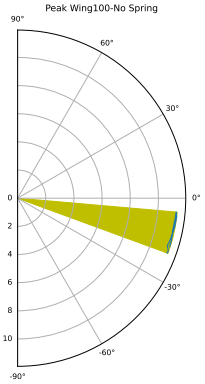
Peak Wing100-No Spring
90°
60°
30°
0°
-30°
-60°
-90°
0
2
4
6
8
10

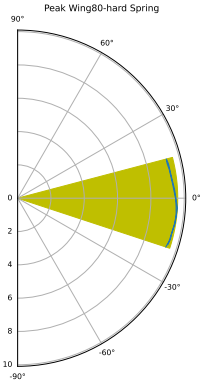
Peak Wing80-hard Spring
90°
60°
30°
0°
-30°
-60°
-90°
0
2
4
6
8
10

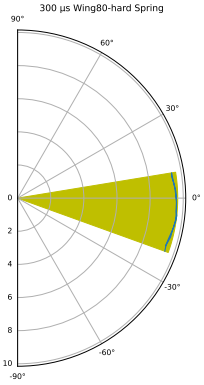
300 µs Wing80-hard Spring
90°
60°
30°
0°
-30°
-60°
-90°
0
2
4
6
8
10

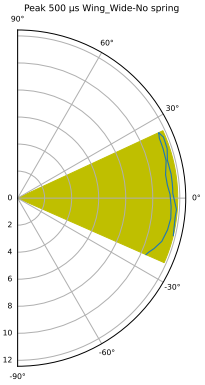
Peak 500 µs Wing_Wide-No spring
90°
60°
30°
0°
-30°
-60°
-90°
0
2
4
6
8
10
12

DEPARTMENT OF MECHANICS AND MARITIME SCIENCES
CHALMERS UNIVERSITY OF TECHNOLOGY
Gothenburg, Sweden
www.chalmers.se

CHALMERS